# Optical exposure characterization and comparisons for discharge produced plasma Sn extreme ultraviolet system

**Huatan Qiu**
**Keith C. Thompson**
**S. N. Srivastava**
**Erik L. Antonsen**
University of Illinois at Urbana-Champaign
Department of Nuclear, Plasma and Radiological Engineering
103 S Goodwin Ave.
214 NEL
Urbana, Illinois 61801
E-mail: hqiu@uiuc.edu

**Darren A. Alman**
**Brian E. Jurczyk**
Starfire Industries LIC.
60 Hazelwood Drive
Champaign, Illinois 61820

**D. N. Ruzic**
University of Illinois at Urbana-Champaign
Department of Nuclear, Plasma and Radiological Engineering
103 S Goodwin Ave.
214 NEL
Urbana, Illinois 61801

**Abstract.** A critical issue for EUV lithography (EUVL) is the minimization of collector degradation from intense plasma erosion, debris deposition, and hydrocarbon/oxide contamination. Collector optics reflectivity and lifetime heavily depend on surface chemistry and interactions between fuels and various mirror materials, such as silicon, in addition to high-energy ion and neutral particle erosion effects. As a continuation of our prior investigations of discharge-produced plasma (DPP) and laser-produced plasma (LPP) Xe plasma interactions with collector optics surfaces, the University of Illinois at Urbana–Champaign (UIUC) has analyzed collector samples before and after exposure in a Sn-upgraded Xtreme Technologies EUV source. Sn DPP postexposure characterization includes multiple samples, Si/Mo multilayer film with normal incidence, 200-nm-thick Ru film with grazing incidence, as well as a Gibbsian segregated (GS) Mo-Au alloy developed on silicon using a dc dual-magnetron cosputtering system at UIUC for enhanced surface roughness properties, erosion resistance, and self-healing characteristics to maintain reflectivity over a longer period of mirror lifetime. Surface analysis draws heavily on the expertise of the Center for Microanalysis of Materials at UIUC, and investigates mirror degradation mechanisms by measuring changes in surface roughness and film thickness as well as analysis of deposition of energetic Sn ions, Sn diffusion, and mixing of multilayer. Results from atomic force microscopy (AFM) and auger electron spectroscopy (AES) measurements show exposure effects on surface roughness and contamination. The best estimates of thickness and the resultant erosion measurements are obtained from scanning electron microscopy (SEM). Deposition, diffusion, and mixing effects are analyzed with depth profiles by AES. Material characterization on samples removed after varying exposure times in the XTS source can identify the onset of different degradation mechanisms within each sample. These samples are the first fully characterized materials to be exposed to a Sn-based DPP EUV source. Several valuable lessons are learned. First, hot mirrors exposed to $SnCl_4$ gas will cause decomposition of the gas and build up a contamination layer on the surface. Second, erosion is mitigated to some extent by the simultaneous deposition of material. Third, and most important, Gibbsian segregation works and a thin Au layer is maintained during exposure, even though overall erosion is taking place. This phenomenon could be very useful in the design of a collector optics surface. In addition, we present Sn DPP collector erosion mechanisms and contamination and provide insight into plasma-facing optics lifetime as high-volume manufacturing (HVM) tool conditions are approached.
 [DOI: 10.1117/1.2358124]

Subject terms: collector optics; extreme ultraviolet; discharge-produced plasma; erosion; Gibbsian segregation; contamination.

Paper 06020R received Apr. 5, 2006; revised manuscript received Jun. 22, 2006; accepted for publication Jun. 25, 2006; published online Sep. 28, 2006.

## 1 Introduction

This paper reports on part of the Collector Lifetime and Erosion Project at the University of Illinois at Urbana–Champaign[1–3] (UIUC). The purpose of this work is to examine the effects of Sn ion debris interaction with the primary collector optic in commercial Sn-fueled EUV sources to ascertain the fundamental erosion processes and critical lifetime issues facing high-volume manufacturing (HVM) for EUV lithography (EUVL).

One way to "mitigate" debris is to lessen its effect on reaching the optical elements.[4] This can be done by offering a continually replenished sacrificial layer (due to preferential sputtering) since the flux to the mirrors is primarily

1537-1646/2006/$22.00 © 2006 SPIE

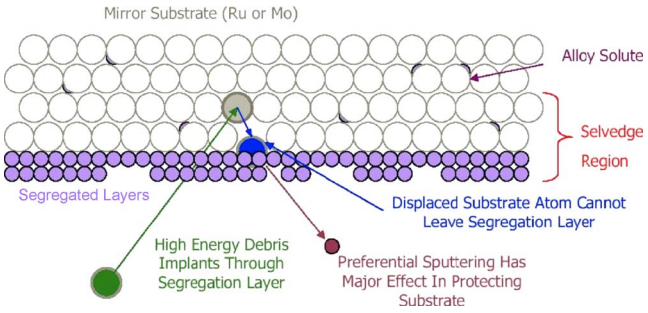


**Fig. 1** Pictorial illustration of surface region effects for preferential sputtering and erosion resistance with GS (from Ref. 4).

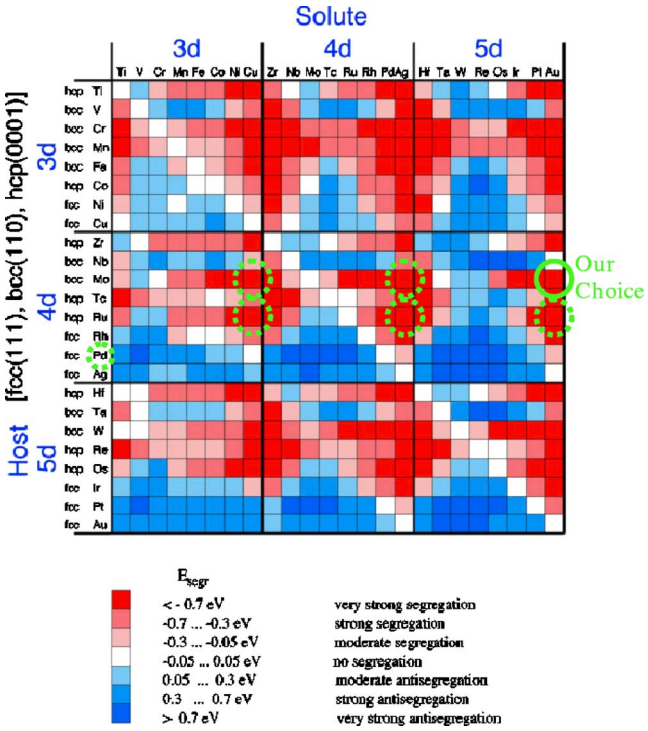


**Fig. 2** Visual representation of segregation energies for various transition metals from Ruban et al.[9]

erosive. Accordingly, an innovative idea using the Gibbsian segregation (GS) concept for EUV collector optic was brought out and tested.

Xe has fallen from favor as the primary candidate for fueling a discharge-produced plasma (DPP) or laser-produced plasma (LPP) EUV source. Sn is now the preferred fuel due to its two to three times higher conversion efficiency[5,6] (CE). However, using Sn as a fuel presents several difficulties—the first and foremost being that Sn atoms will deposit on the mirrors and degrade the reflectivity.

A film with a high reflectivity at 13.5 nm (the wavelength to be used for EUVL) and a high durability against erosion is required to be the collector mirror in EUV applications. Based on the preceding criteria and our prior investigations,[1] three samples are investigated consisting of one Si/Mo multilayer mirror (MLM), a ~200-nm-thick Ru deposited on Si substrate prepared by Saša Bajt at Lawrence Livermore National Laboratory (LLNL), and a ~330-nm-thick GS Mo-Au alloy fabricated by UIUC. The multilayer, termed "ML1," is optimized with 50 bilayer pairs with a period thickness of 4.17 nm Si and 2.78 nm Mo, and has a 2.3-nm Ru capping layer. The UIUC GS alloy is fabricated at Mo-0.56% Au with a 3.6-nm Au capping layer, to prevent the oxidation before exposures. In actual use, this capping layer would quickly be eroded to the thickness on the order of one atomic layer (0.35 nm) to activate the segregation process. All three films are prepared using dc magnetron sputtering technique.

This paper describes the postexposure analysis of three samples, Ru at 20-deg grazing incidence, Si/Mo multilayer at 10-deg normal incidence, and the UIUC GS Mo-Au alloy at 20-deg grazing incidence after "2.2 million" shots from a $SnCl_4$-fueled XTS 13-35 source. This is the first reported work from a commercial Sn source. The GS concept is introduced briefly in Sec. 2. Section 3 discusses the detailed experimental setup and conditions. Surface characterization for both pre- and postexposure are performed to investigate mirror degradation mechanisms by measuring changes in surface roughness and thickness as well as contamination, erosion, and debris mitigation scheme are discussed in detail in Sec. 4.

## 2 GS Concept

GS has been defined as an observed phenomenon[7] such that the tendency of certain solute elements in a homogenously interspersed solid solution will tend to accumulate at imperfections, such as grain boundaries and interfaces, in the bulk lattice and may segregate to the free surfaces. Since many important processes and phenomena occur at the surface, there is the potential for functional surface engineering to achieve desired physical (sputtering, roughness, and thermal), chemical (oxidation resistance and binding), electrical (resistivity), and optical (reflectivity) effects. The primary mechanism of surface enrichment is diffusion of one species through the bulk material, without concerning the contribution of the absorption from the ambient background. The application of GS to 13.5-nm EUV optics would be to engineer the surface for enhanced surface roughness properties, erosion resistance, and self-healing characteristics to maintain reflectivity over a longer period of mirror lifetime.

Theoretically, the sputter depth—or the characteristic length the sputtered atoms are sputtered from—is about a few monolayers (0.2 to 1 nm) of material, while the EUV reflection properties are associated with 1 to 2 wavelengths into the material, 13.5 to 27 nm. EUV light operated at a wavelength of 13.5 nm is generated by *z*-pinch with either a DPP or an LPP EUV source. Both include many types of energetic ion debris during the plasma pinch. Therefore, optical EUV mirrors will experience significant energy deposition, due to the absorption of the EUV light and the bombardments by the energetic ion debris from the source, potentially greater than 10 kW incident light in HVM tool conditions. Then, there will be ample energy, together with the bombardments by the energetic ion debris, to drive GS processes at the surface.

As shown[4] in Fig. 1, some segregated surface atoms are preferentially sputtered, while displaced Mo atoms by high-

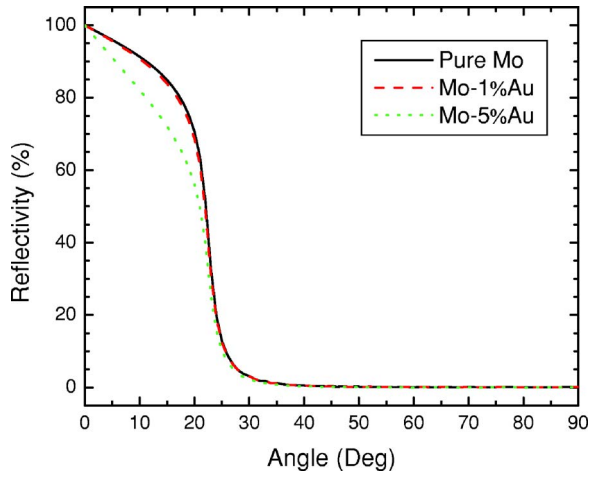


**Fig. 3** Reflectivity calculation as the function of grazing angle for 13.5-nm EUV light for pure Mo and different Mo-Au GS configurations. The film is set at 200 nm thick on the Si substrate with 1-nm root mean square (rms) surface roughness.

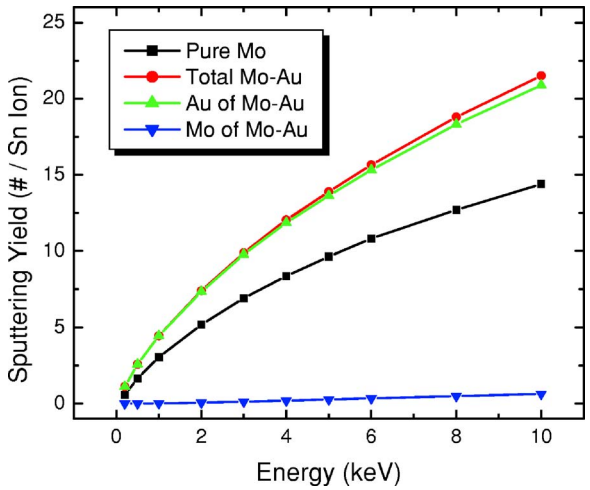


**Fig. 4** SRIM calculations for sputtering yield at 20-deg Sn grazing incidence for pure Mo and Mo-1% Au with a segregated 0.5-nm Au capping segregated layer.

energy debris from the bulk material are trapped inside the bulk without tunneling due to the segregated capping layer. The selvedge and near-surface characteristics are important for estimating the EUV reflectivity for total external reflection, which must be satisfied for reflection with minimal attenuation in the bulk material. There are binary, ternary, and quaternary alloy configurations to maximize the surface binding energy, to provide sacrificial material (to be lost due to preferential sputtering), and/or to enhance thermodynamic transport properties for regenerative healing. The surface mole fractions will depend on the free-energy minimization between the host and solute elements.

One Gibbsian configuration is to alloy the optical material with a preferential sputtering solute that would be displaced during bombardment of high-energy ions. This "sacrificial sputtering" characteristic could maintain the high-reflectivity substrate with low surface roughness characteristics for longevity. For example, high-reflection Mo could be alloyed with a massive segregating material, such as Au ~1%, to form a shallow high-surface-energy layer to protect the reflection layer (Mo). Alloy and segregation layer combinations could be selected with self-healing diffusion and migration processes to repair surface damage under enhanced surface segregation due to radiation energy bombardment.

**Table 1** SRIM sputtering yield calculations for Mo-1% Au GS alloy.

| | Sputtering Yield | | | | | |
|---|---|---|---|---|---|---|
| Energy (keV) | Pure Mo | Total Mo-Au | Solute Au of Mo-Au | Host Mo of Mo-Au | $Y_{solute}/Y_{Mo}$ | Reduction from Pure Mo (%) |
| 0.2 | 0.5532 | 1.102 | 1.10 | 0.00001 | — | 100.0 |
| 0.5 | 1.648 | 2.571 | 2.57 | 0.00137 | 1875.91 | 99.9 |
| 1 | 3.043 | 4.450 | 4.44 | 0.0108 | 411.11 | 99.6 |
| 2 | 5.173 | 7.401 | 7.35 | 0.055 | 133.64 | 98.9 |
| 3 | 6.917 | 9.882 | 9.77 | 0.1155 | 84.59 | 98.3 |
| 4 | 8.372 | 12.035 | 11.85 | 0.1845 | 64.23 | 97.8 |
| 5 | 9.633 | 13.892 | 13.63 | 0.2621 | 52.00 | 97.3 |
| 6 | 10.812 | 15.657 | 15.32 | 0.3337 | 45.91 | 96.9 |
| 8 | 12.693 | 18.798 | 18.32 | 0.4805 | 38.13 | 96.2 |
| 10 | 14.389 | 21.51 | 20.89 | 0.6216 | 33.61 | 95.7 |

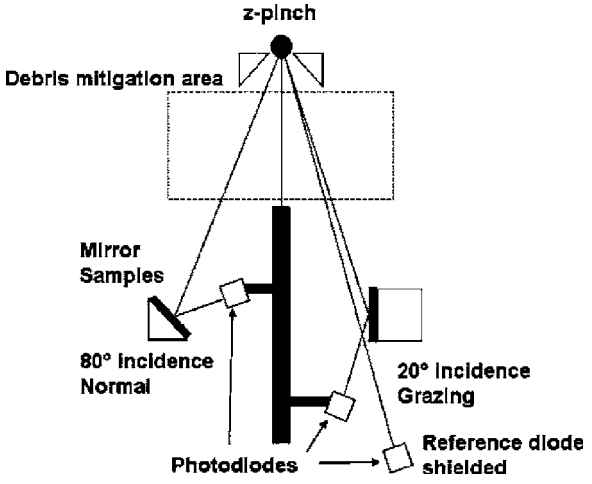


**Fig. 5** Schematic of XCEED DPP EUV exposure setup and working process (from Ref. 15).

The reflectivity of grazing incidence collectors mainly depends on the material, its smoothness, and the angle of incidence. In detail, the mirror material will determine the base reflectivity. A low surface roughness will minimize the unexpected diffraction and diverging reflection. The angle of incidence is to govern the sputtering of the debris impact. In addition, the oxidation of the mirror surface will dramatically decrease the reflectivity and lifetime of the mirror optics.[8] Most high-reflectivity materials, e.g., Mo, are likely to grow with columnar grains or fiber textures. These features will also decrease the reflectivity. Commercially, the longevity before replacing a new set of collectors in HVM is necessary to increase the productivity and lower the cost of ownership (COO). Our GS alloy is proposed to be used as a grazing incidence collector mirror, which will take into consideration all of the preceding aspects.

Currently, the three leading EUV reflective materials employed by source suppliers and optics companies are ruthenium (Ru), palladium (Pd), and molybdenum (Mo). From the literature, the surface segregation energy in transition-metal alloys is governed by the difference in surface energies of the pure alloy components, the surface segregation energies, and the crystal structure of the alloy components. The segregation energies and processes for Mo, Ru, and Pd elements were detailed by Ruban et al.[9] A highlighted colorful matrix of these energy levels is visually depicted in the Fig. 2, copied from Ruban et al.[9] Correspondingly, it indicates the strongest segregation of Mo-Au configuration. In addition, the oxidation resistance is another critical factor for the reflectivity of a collector mirror. Therefore, Mo-Au became the final candidate for our GS alloy.

Initial calculations on the reflectivity and preferential sputtering were performed for the Mo-Au GS alloy to test its effectiveness as a grazing incidence collector used for EUVL.

### 2.1 *Reflectivity Calculation*

The three key factors affecting the reflectivity of grazing incidence collector mirrors are the materials, its surface smoothness, and the angle of incidence. Available data enable one to calculate the x-ray or EUV reflectivity of a mirror material of your choice for a variety of wavelengths and angles of incidence.[10,11] Initial code investigations of a hypothetical 100% segregated, 13.5-nm EUV-oriented GS alloy were performed by this reflectivity evaluation program. The GS alloys are assumed to be Mo alloy with 1 and 5% Au, respectively. The grazing incidence collector consists of a number of internested shells; each utilizing angles from approximately 10 to 20 deg. In this paper, our experimental configuration for grazing incidence is setup at 20 deg. Thus, the reflection at 20 deg is used as a scalar metric to judge the effectiveness of a given collector.

Figure 3 shows the variation of reflectivity as a function of grazing angles using available data[10,11] for different Mo-Au GS configurations and then compared with reflectivity from pure Mo film. Note that the reflectivity for pure Mo film at 20° is 70.6%. The results indicate that there is a slight reduction in reflectivity due to the presence of the surface-segregated layer. For the reference case of Mo-1% Au, the reduction from pure Mo is only $\leqslant$2.8%, depending on the angle of incidence. Note that higher Au content can lead to greater reflectivity loss. A sample with 5% Au has a base reflectivity at 20 deg of only 56.1% compared to 68.5% for 1% Au. Those values are for a 200-nm thickness and 1-nm rms surface roughness. In theory, the reflectivity reduction from a carefully fabricated GS alloy configuration (lower alloy ratio of Au component) is comfortably accepted.

### 2.2 *Preferential Sputtering*

A quick erosion estimate was made using the standard binary collision code, SRIM, or the Stopping and Range of Ions in Matter.[12] A representative test surface was created


(a) (b) (c)

**Fig. 6** Surface contamination pictures of the exposed samples; (a) ML1 after gas-blow-off cleaning and before liquid cleaning; (b) ML1 after all cleaning; (c) SEM top view of the contamination layer of the Mo-Au sample.

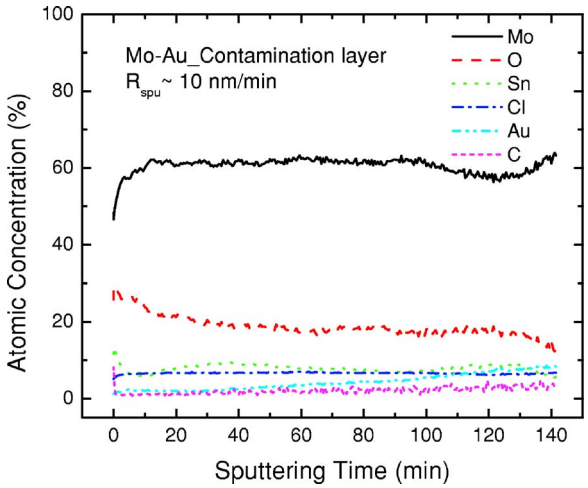


**Fig. 7** AES depth profiling of the contamination layer of the postexposed Mo-Au sample.

according to the hypothetical 100% segregated Mo-Au alloy used in previous reflectivity investigation. This is actually a 200-nm-thick Mo-1% Au bulk material with a 0.5-nm Au capping segregated layer. For comparison, another 200-nm-thick pure Mo film was created and tested. Sputtering yields were calculated for Sn incident ranging from 200 eV to 10 keV and 20-deg grazing incidence on the surfaces already described. The results are shown in Fig. 4 and Table 1.

Initial estimates of the effect of segregated layers on the lifetime of an ideal segregated surface are impressive. For the case of a pure Mo collector surface with EUV incident at 20-deg grazing, 200 eV to 10 keV $Sn^+$ ions (emitted from the $z$-pinch during maximum compression) will sputter approximately up to 14.4 Mo atoms per incident ion. The presence of 0.5 nm of Au on top of the Mo as a sacrificial layer reduces the Mo sputtering yield to 0.6 even at 10 keV, and thus effectively shields the mirror surface from ion damage. As displayed quantitatively in Table 1, the Mo-1% Au GS alloy shows a significant ($\geqslant$95.7%) reduction in Mo erosion over the pure Mo film, reducing the Mo sputtering yield to about 4% of its initial value. The preferential sputtering process occurs even at 10 keV Sn impact energies and is illustrated in Fig. 1. Eventually, the Mo-Au GS alloy would perform best under irradiation conditions for least Mo sputtering.

These results indicate that if the regenerative transport processes (bulk, grain, interface diffusion) and surface renormalization are faster than the erosion time scale (i.e., the average time between large energy sputtering events), then the collector optic could be self-repairing. However, there are still many unanswered questions, such as the effect of surface roughness, the ability of material to segregate through impurities, and whether an easily diffusible sacrificial alloy material that is only one or two atoms thick would indeed offer superior lifetime. Projected experiments are underway to setup and test this concept.

## 3 Experimental Exposure

The Xtreme Commercial EUV Emission Diagnostic (XCEED) experiment is designed to investigate characterization of the DPP source fueled with Xe and Sn, the emitted debris fields, along with optical mirror exposure to the pinch plasma source. The XCEED utilizes a XTS 13-35 source, which was recently upgraded to produce EUV light from Sn ions. This is accomplished by flowing $SnCl_4$ into

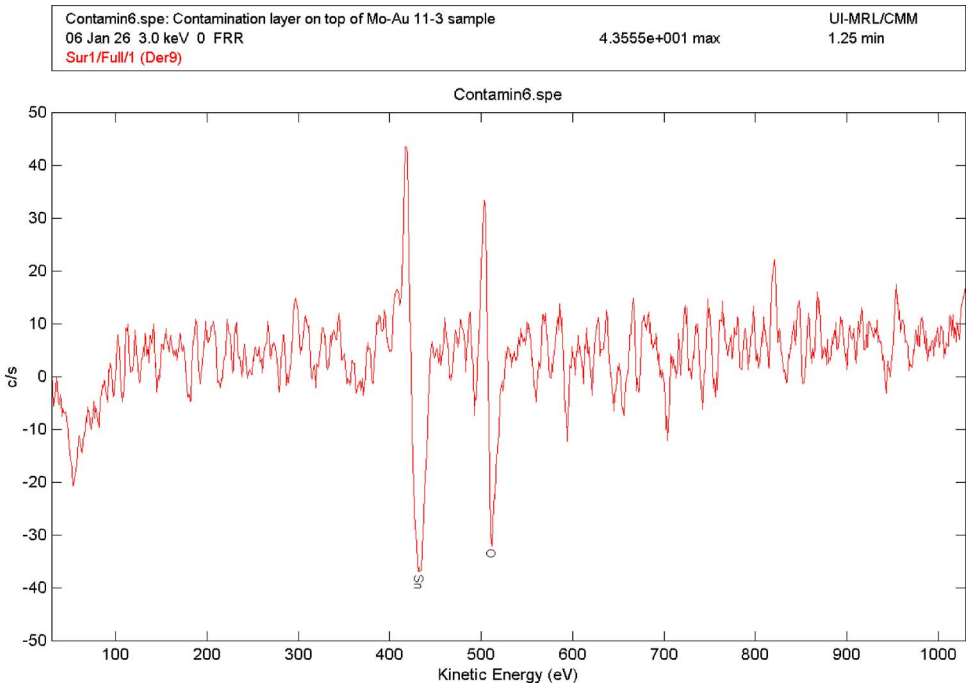


**Fig. 8** Surface analysis at 205.8 min (~1.23 $\mu$m) of the second run of AES depth profiling of the contamination layer of the postexposed Mo-Au sample.

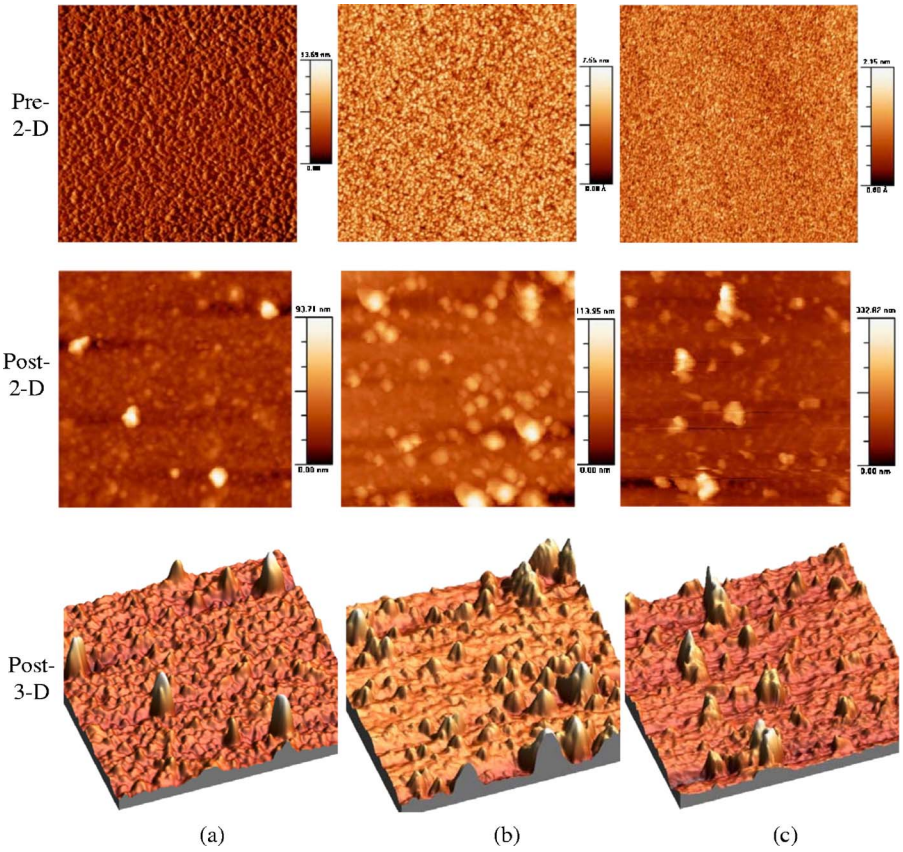


**Fig. 9** AFM results with scan size at $2\times2$ $\mu$m: (a) Mo-Au at grazing incidence, (b) Ru at grazing incidence, and (c) ML1 at normal incidence.

the pinch region instead of Xe. The XCEED experimental efforts are performed to characterize a commercial-scale DPP EUV source, including fast ion debris, debris mitigation techniques for damage of collector mirrors, and exploring the characteristics and the erosive effects on the collector mirror surfaces after the DPP EUV exposures. The samples were characterized by microanalysis measurements using atomic force microscopy (AFM), auger electron spectroscopy (AES), and scanning electron microscopy (SEM) techniques. The former experiments are detailed elsewhere,[13–15] and the latter are presented in this paper.

The DPP EUV exposure setup and working process is shown in Fig. 5. The chamber enables characterization of optic samples at varying exposure times for normal and grazing incidence reflection angles. All DPP mirror samples discussed here are placed 28 cm from pinch and exposed for 2.2 million pulses (64-min exposure) with debris mitigation present. ML1 is exposed at normal incidence (mirror plane is ~80 deg to the incoming light vector), while Ru and GS Mo-Au are exposed at ~20-deg grazing incidence. The DPP exposure is operated at 575 Hz pinch frequency with 35 W over $2\pi$ sr output EUV light (2% bandwidth) power. The ellipsoid pinch geometry is $\sim1.5\times0.5$ mm. The XTS 13-35 source is equipped with a foil trap-based debris mitigation tool with Ar buffer gas flow, which is designed to slow or remove fast ions etc. For this Sn-fueled DPP experiment, only 37.5% of maximum buffer gas was used. The chamber pressure during operation is 2 mTorr with Sn feed gas and the Ar as both carrier and buffer gas.

## 4 Results and Discussion

### 4.1 *Surface Contamination*

After 2.2 million shot exposure and 2 h of cooling time, the samples were taken out from the XCEED chamber. The immediate surface looked thick and was covered with a dark-gray contamination layer. After a couple of hours, most of the contamination layer of the Ru sample flaked off by itself. Any remaining contamination layer was blown off by pressurized $N_2$ gas leaving a fairly clean surface for further characterization. Before analysis, the Mo-Au sample was also cleaned by blowing pressurized $N_2$ gas, however, in this case, only the central part of contamination layer was removed. Cleaning through a blow gas did not quite work for the ML1 sample, as shown in Fig. 6(a). Afterward, as the samples were open for analysis, liquid droplets of a dark green color were mixed with the contamination layer. A possible guess is that the contamination layer was hydrated, and that the cold temperature dropped the hydration layer below its dew point, thereby desorbing the water into droplets. This was confirmed in part by rinsing the samples with deionized (DI) water. The contamination was then removed. Figure 6(b) shows a picture of ML1 sample after DI water cleaning. It is not perfectly clean as no clear film surface can be seen, but at least it is a mirror

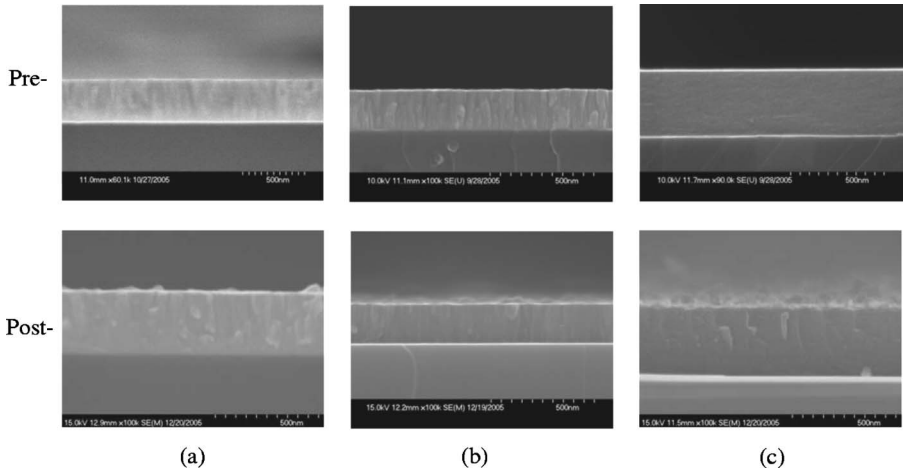


**Fig. 10** SEM results of cross-sectional views: (a) Mo-Au at grazing incidence, (b) Ru at grazing incidence, and (c) ML1 at normal incidence.

film and can be analyzed under AFM and AES. To visualize the contamination layer, a SEM picture of the contamination surface of the Mo-Au sample is shown in Fig. 6(c). The fully covered grain structure of the contamination layer might block any possible reflection. Obviously, the films could not be perfectly cleaned by blowing gas or by the use of DI water. As a result, it increased the difficulty of measuring the roughness of the actual film surface. Therefore, the AFM measurement of ML1 can not be trusted as the actual film surface roughness, since the contamination layer was not well removed to show the clear film surface. However, the AFM measurements of the Ru and Mo-Au samples should be trustworthy to a reasonable order of magnitude.

Several questions arise from the AES analysis for the contamination issue concerning the composition of the contamination and its origin. The major question of interest concerns the time of contamination formation. It is highly important and desirable to understand whether they were formed before the EUV exposure or after the exposures were performed. This will be the key to understanding whether the samples were really contacted and interacted with the ion debris during Sn-DPP EUV exposure. The surface analysis of pre-and postexposed samples provides the answer and is explained to the best of our understanding in the following sections.

A preliminary investigation of the surface contamination was performed by AES via depth profiling. The detailed composition and depth profile information is shown in Fig. 7. A rough estimate of the thickness of depth profile is $\sim 1.4\ \mu$m, which is much thicker than the Mo-Au film thickness ($\sim 330$ nm). However, the Mo and O components remain at relatively steady high levels. This implies that the contamination layer is less likely to form before plasma exposure. If the contamination layer was present before the plasma exposure, the Mo component of the film would be shielded by this layer and the Mo traces would not be observed during AES; that is, the film did interact with the EUV exposure and ion debris. This is also proved by the erosion measurements with SEM, as explained in Sec. 4.3. Also, the contamination possibly includes oxidations, in particular, for Mo-include samples. Ru is largely immune to atmospheric attack, which might be the reason why the contamination layer of Ru was stripped off easily.

The second AES depth profile investigation, specifically for the contamination layer of postexposed Mo-Au sample, was performed and paused at 205.8 min and the surface analysis was performed with an approximately 6 nm/min sputtering rate. At this position, the contamination depth was calculated to be around 1.23 $\mu$m. Figure 8 shows the surface survey, where the Sn and O peaks are clearly distinct, together with tiny Mo peaks. This makes possible the conclusion that the contamination is a result of Sn-oxidation. While the base pressure is in the $10^{-8}$ Torr range inside the chamber, 2 h of cooling time is quite sufficient for some background oxygen and water vapor to react with the surface as well. Another possible reason is that the samples were not cooled enough to avoid oxidation when exposed to open air, which explains why we see a large proportion of O in AES surface survey at the $\sim 1.23$-$\mu$m depth. Note that we do not find Cl, which leads to the conclusion that the contamination is not directly from the $SnCl_4$ fuel but it is possibly a result of Sn redeposition on the surface or slight Sn implantation into the surface. To keep the substrate free from Sn and Cl, it is important to continue to bombard the surface with ions and heat the mirror at the same time to avoid the possibility of Sn deposition.

From these results, we conclude that the contamination formed after the exposure and consisted of oxidation and Sn due to redeposition or implantation. Note that these contamination issues would also be faced in an HVM environment any time the tool was stopped. Further understanding and innovative solutions will be the subject of our future work.

### 4.2 *Surface Roughness*

Surface roughness can limit the reflectivity of surfaces, particularly in the case of a grazing incidence collector. To investigate how the exposures affected the samples in this regard, AFM is used to measure surface height variations over several different lateral length scales. Scans are performed over $5\times 5$-, $2\times 2$-, $1\times 1$-, and $0.5\times 0.5$-$\mu m^2$ areas.

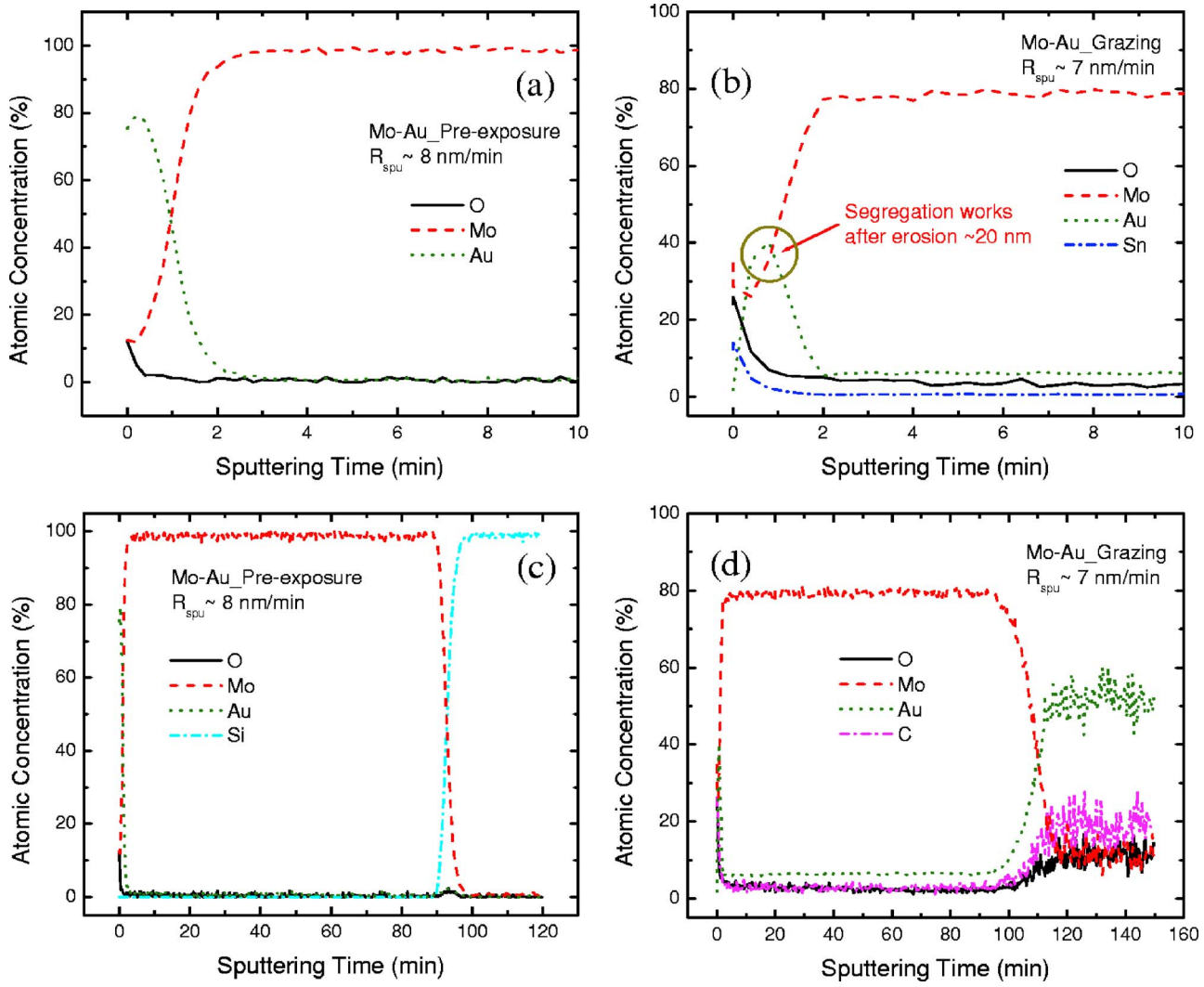


**Fig. 11** AES results of depth profiling of Mo-Au sample: (a) and (c) preexposure and (b) and (d) postexposure. (a) and (b) show the first 10 min of depth profiling of (c) and (d).

The examples shown in Fig. 9 are $2 \times 2$-$\mu m^2$ AFM scans of three samples before and after exposure in the Sn-DPP source.

Figure 9 shows the AFM results of pre- and postexposed samples. The 3-D pictures of AFM surface scan are shown to compare with the 2-D views and determine the important features. The rms roughness of postexposure samples is clearly larger than that of the preexposure samples. However, there are many "huge" islands on the surfaces of each sample, as seen in the 3-D pictures, which result in the "huge" rms roughness (especially for ML1), while the rest of the surface remains relatively smooth. Considering the impact of contamination layer, the actual film surface should be smoother than the current result. Actually, the contamination residue can be seen on top of the samples (see Fig. 6), especially for ML1. Therefore, it is reasonable to attribute the "huge" roughness to the surface contamination (as discussed in Sec. 4.1) instead of the impact of ion debris. Assuming that the contamination layer formed after the completion of the exposure, it is comfortable to say that the surface roughness will be smoother (or much smoother for ML1) than the current results if we can solve the contamination issue.

Table 2 summarizes the AFM results, giving the calculated rms roughness and the change ratio values for each of

**Table 2** AFM results for preexposed and Sn-DPP-exposed samples.

| | rms Roughness (nm) | | |
|---|---|---|---|
| Material | Preexposure | Postexposure | Change (post/pre) |
| Mo-Au | 1.790 | 7.888 | 4.4 |
| Ru | 1.030 | 12.441 | 12.1 |
| ML1 | 0.242 | 32.386 | 133.8 |

the three samples. The Mo-Au has the less roughness change 4.4× compared with the Ru sample 12.1×, considering that they received similar cleaning treatments and same exposure condition, at grazing incidence. One possible reason might be the segregation effect of our Mo-Au segregation alloy. Actually the top Au capping layer (~ a few nanometers) in our Gibbsian alloy quickly sputters away during the initial exposure until a few atomic monolayer's remain, and then the Au segregates onto the surface along the grain boundary to refresh the surface removal due to sputtering by ion flux. This segregation will play two important roles. One is to protect the mirror material (Mo) underneath the Au surface layer by sacrificial sputtering. Another is to repair the surface damage due to the bombardments by ion debris. We believe this segregation effect is beneficial and is the reason why the Mo-Au segregation alloy has the smallest roughness change, since the AES result in Sec. 4.4 prove that the segregation effect indeed takes place.

### 4.3 *Film Thickness and Erosion*

The best measurements of film thickness is obtained using cross-sectional SEM, since the thickness estimates obtained by depth profiles in a technique such as AES are not reliable due to the varying sputtering rate in the AES instrument. Figure 10 shows SEM film cross sections for three pre- and postexposed samples in the Sn-DPP source. Table 3 summarizes the thickness measurements and erosion derived from the cross sections. When compared to thickness estimates made on the pre-exposed samples, erosion of between 3 and 20 nm is seen.

The top surfaces in the cross-sectional pictures of the postexposure samples are not as clear as those of the preexposure samples. Large fragments can be seen almost everywhere on the rough surface, which indicates the contamination layer. This made the accuracy of the thickness measurement (erosion) a little worse. However, erosion still can be seen, according to the Table 3. The fact that erosion is seen is further evidence that the contamination layer forms after the exposure and it did not prevent the erosion. It is interesting that the Mo-Au is eroded most, while its roughness change is the least. The contribution of the segregation effect could be the answer. It appears that the Au may indeed act as a sacrificial layer protecting the active mirror component.

**Table 3** SEM thickness measurements for preexposed and Sn-DPP-exposed samples.

| | Thickness (nm) | | |
|---|---|---|---|
| Material | Preexposure | Postexposure | Erosion (nm) |
| Mo-Au | 330 | 310 | 20 |
| Ru | 192 | 189 | 3 |
| ML1 | 353 | 343 | 10 |

### 4.4 *Film Compositions and Segregation Evidence*

#### 4.4.1 *Gibbsian segregation*

AES is used to investigate the film composition and depth profiling before and after exposure. Figure 11 shows the AES depth profiles of the pre- and postexposed Mo-Au sample. Figure 11(b) shows that the Au component is higher than Mo component in the initial few nanometers of the eroded Mo-Au film. The bulk concentration of Au in the Mo-Au alloy is ~0.56%, while ~40% (or higher if a smaller sputtering interval is used during AES depth profiling) Au is found at the film surface even after being eroded by ~20 nm. This clearly proves our GS idea. It is exciting to see segregation work for our Mo-Au segregation alloy. Another notable phenomenon is that Au also diffuses to the boundary between the Mo and the Si substrate, as seen in Fig. 11(d). In future work, a diffusion barrier layer might be

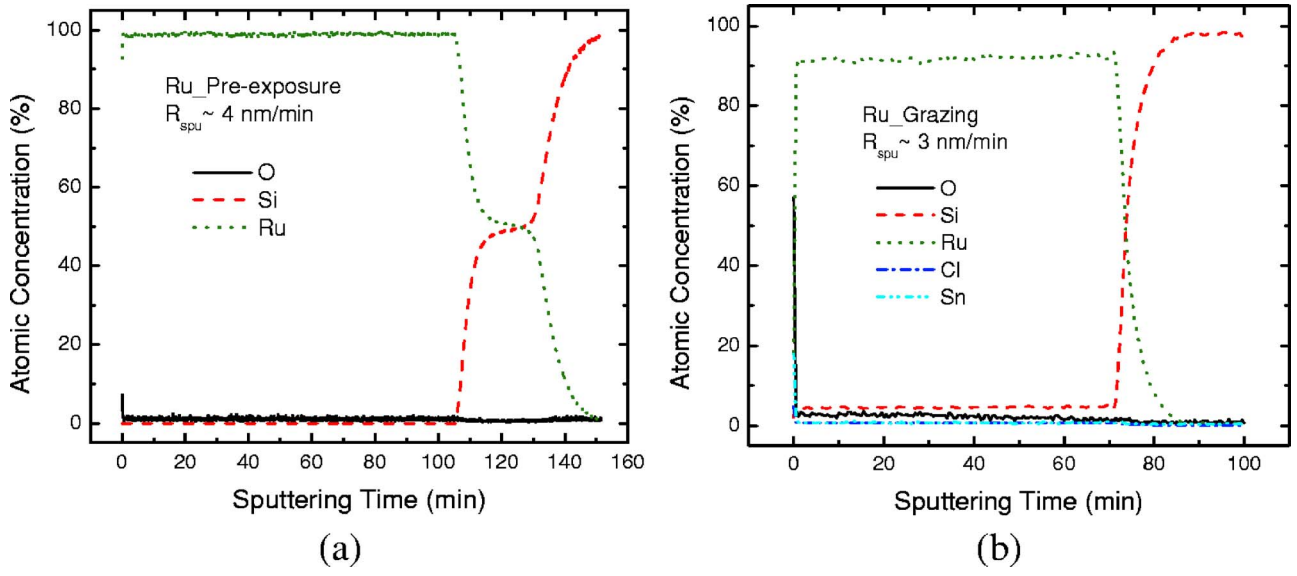


**Fig. 12** AES results of depth profiling of Ru sample: (a) preexposure and (b) postexposure.

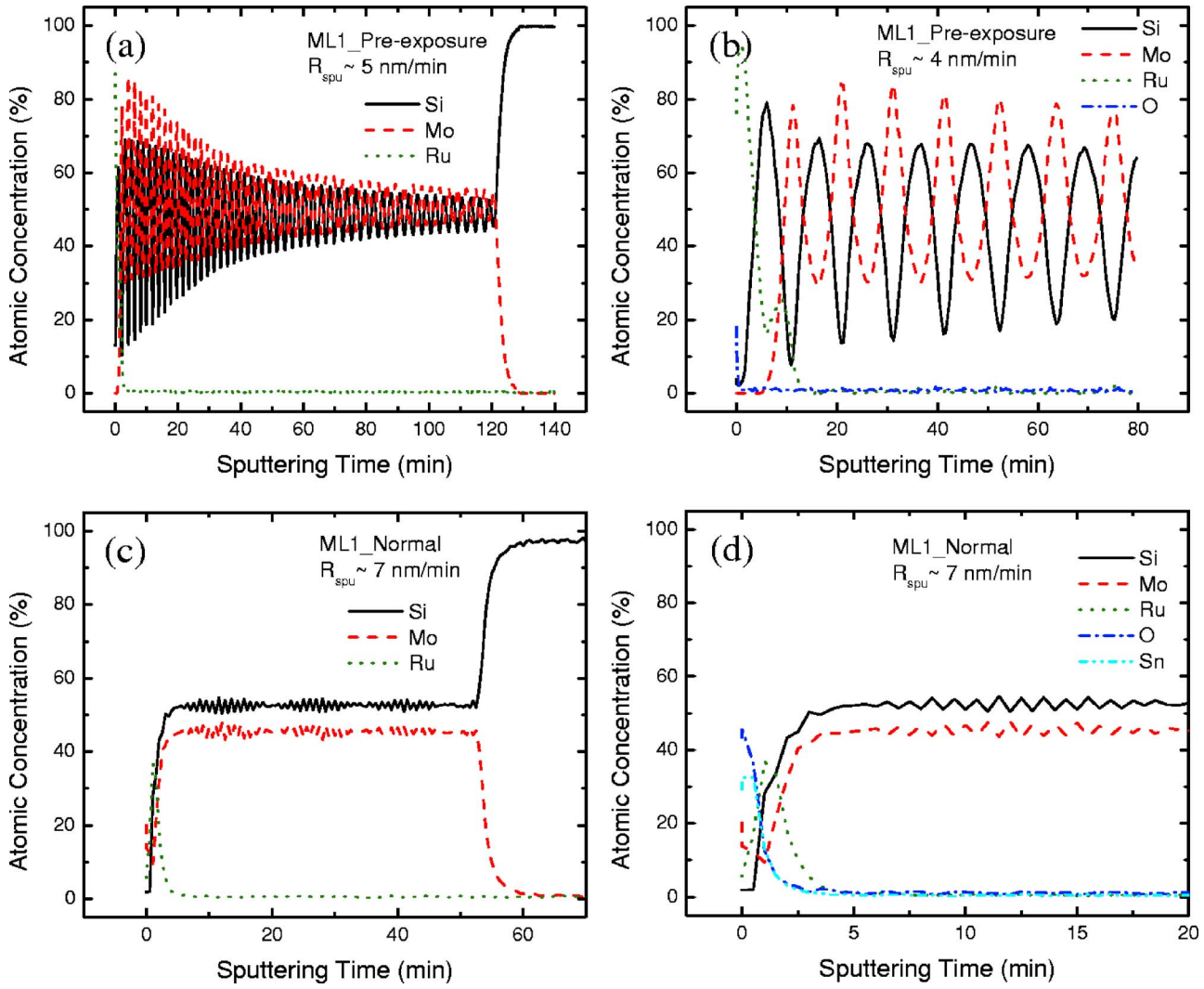


**Fig. 13** AES results of depth profiling of the ML1 sample: (a) and (b) preexposure and (c) and (d) postexposure.

helpful to prevent the drain of Au to the Si substrate and interface, where, there will be more Au to refresh the surface and protect the optical mirror material.

### 4.4.2 *Composition and depth profiling*

Figure 12 shows the AES depth profiles of the pre- and postexposed Ru sample. Ru pre- and postexposure profiles are almost the same except for the Sn and Cl, as seen on the very top surface. Note that only ~3 nm is eroded. Deposition of Sn and Cl from the pinch may balance the erosion from the Sn and Cl ions to some extent.

Figures 13(a)–13(d) show the AES depth profiles of the pre- and postexposed ML1 sample. Unfortunately, a large ion beam size and long sputtering intervals are required because the thickness of the contamination layer could not be estimated. As a result, the sputtering interval was not small enough to achieve a fine resolution, as shown in Figs. 13(c) and 13(d). Therefore we did not see the intersection of the Mo and Si curves, which clearly indicates the Mo/Si bilayer structures in the depth profiles of the postexposure ML1, though those layers are definitely present. In addition, the Ru capping layer is still quite prominent in the postexposure depth profiles. However, this signal may be due to a C component from the contamination layer since their peak overlaps. This is very important to show when the contamination layer formed. If it is a C component, then the contamination layer formed after exposure. If it is a Ru component, then at least some of the contamination layer formed at the initial stage and prevented film erosion from the plasma. Future work will investigate this phenomenon. Remember that the ML1 sample had a "stubborn" contamination layer in addition to the easy-to-remove postexposure contamination layer that the other two surfaces possessed. Independent of that question, Sn and Cl components showed up on the surfaces of all samples, showing that Sn and Cl deposit on as well as erode off the surfaces of these mirrors.

## 5 Conclusions

Three samples (Mo-Au, Ru, and ML1) were exposed to 2.2 million shots in the XCEED Sn-DPP source at UIUC, at a 575-Hz pinch frequency with a debris mitigation tool present. Pre- and postexposed samples were analyzed at the Center for Microanalysis of Materials at the University of

Illinois. The techniques performed included AFM, SEM, and AES. AFM gave the surface roughness. SEM provided the best estimates of film thickness and erosion. Finally, AES measured the elemental composition of the samples versus depth.

The contamination issue is a serious problem as it fully covered the exposed samples. There is a need for better understanding and an effective removal solution to the contamination problem. The contamination layer formed after the completion of the exposure and consisted of oxidation and Sn due to redeposition and implantation. GS alloy Mo-Au was eroded most, while its surface roughness change was the least. This is because of the self-healing nature of the alloy by refreshing and repairing the damaged surface through GS diffusion along grain boundary.

These samples were the first fully characterized materials exposed to a Sn-based DPP EUV source. Several valuable lessons were learned. First, hot mirrors exposed to $SnCl_4$ gas cause decomposition of the gas and build up a contamination layer on the surface. Second, erosion is mitigated to some extent by the simultaneous deposition of material. Third, and most important, GS really works and a thin Au segregated layer is maintained during exposure, even though overall erosion is taking place. This phenomenon could be very useful in the design of a collector optics surface.

Furthermore, even for the case of condensable fuels such as Li or Sn, the use of GS collector optics may indeed be useful. In that case, the key would be to find a segregant that has either (1) a high etch selectivity with respect to the etching of the condensable fuel, (2) a low sputtering coefficient if the removal is accomplished by ion bombardment, or (3) a low vapor pressure if the removal is accomplished by evaporation.

## Acknowledgments

The authors would like to thank Intel and Sematech for their kind support. We are thankful to Xtreme Technologies GmbH in Göttingen, Germany, for partially providing us the current EUV source and for their technical help from time to time as needed. A portion of this research was carried out in the Center for Microanalysis of Materials, University of Illinois, which is partially supported by the U.S. Department of Energy under Grant No. DEFG02-91-ER45439.

## References

1. H. Qiu, D. A. Alman, K. C. Thompson, J. B. Spencer, E. L. Antonsen, B. E. Jurczyk, D. N. Ruzic, and T. P. Spila, "Characterization of collector optic material samples before and after exposure in laser produced plasma and discharge produced plasma EUV sources," *J. Microlithogr., Microfabr., Microsyst.* **5**, 033006 (2006).
2. D. A. Alman, H. Qiu, T. P. Spila, K. C. Thompson, E. L. Antonsen, B. E. Jurczyk, and D. N. Ruzic, "Characterization of collector optic material samples exposed to a DPP EUV light source," submitted for publication.
3. H. Qiu, K. C. Thompson, S. N. Srivastava, E. L. Antonsen, D. A. Alman, B. E. Jurczyk, and D. N. Ruzic, "Optical exposure characterization and comparisons for Sn EUV systems," *Proc. SPIE* **6151**, 1281 (2006).
4. D. N. Ruzic, "Origin of debris in EUV sources and its mitigation," in *EUV Sources for Lithography*, Ch. 36, Vivek Bakshi, Ed., SPIE Press, Bellingham, WA (2006).
5. U. Stamm, "Extreme ultraviolet light sources for use in semiconductor lithography-state of the art and future development," *J. Phys. D* **37**, 3244–3253 (2004).
6. V. M. Borisov, A. I. Demin, A. V. Elstov, A. S. Ivanov, Y. B. Kiryukhin, et al., "Xenon and tin pinch discharge sources," Chap. 16 in *EUV Sources for Lithography*, Vivek Bakshi, Ed., SPIE Press, Bellingham, WA (2006).
7. P. A. Dowben and A. Miller, *Surface Segregation Phenomena*, CRC Press, Boca Raton, FL, (1990).
8. S. Bajt et al., "Design and performance of capping layers for extreme-ultraviolet multilayer mirrors," *Appl. Opt.* **42**, 5750–5758 (2003).
9. A. V. Ruban, H. L. Skriver, and J. K. Norskov"Surface segregation energies in transition-metal alloys," *Phys. Rev. B* **B59**, 15990–16000 (1999).
10. http://www-cxro.lbl.gov/optical_constants/.
11. B. L. Henke, E. M. Gullikson, and J. C. Davis, "X-ray interactions: photoabsorption, scattering, transmission, and reflection at E =50–30000 eV, Z=1–92," *At. Data Nucl. Data Tables* **54**, 181–342 (1993).
12. J. F. Ziegler, J. P. Biersack, and U. Littmark, *The Stopping and Range of Ions in Solids*, Pergamon, New York (1985).
13. E. L. Antonson, K. C. Thompson, M. R. Hendricles, D. A. Alman, B. E. Jurczyk, and D. N. Ruzic, "Ion debris characterization from *z*-pinch extreme ultraviolet light source," *J. Appl. Phys.* (in press).
14. E. L. Antonson, K. C. Thompson, M. R. Hendricles, D. A. Alman, B. E. Jurczyk et al., "XCEED: XTREME commercial EUV exposure diagnostic experiment," in *Emerging Lithographic Technologies IX*, *Proc. SPIE* **5751**, 1192–1202 (2006).
15. K. C. Thompson, E. L. Antonson, M. R. Hendricles, B. E. Jurczyk, M. Williams, and D. N. Ruzic, "Experimental test chamber design for optics exposure testing and debris characterization of a xenon discharge produced plasma source for extreme ultraviolet lithography," *Microelectron. Eng.* **83**, 476–484 (2006).

Biographies and photographs of authors not available.